doi:10.1016/j.jmb.2011.01.019 J. Mol. Biol. (2011) 407, 284–297

Contents lists available at www.sciencedirect.com

Journal of Molecular Biology

journal homepage: http://ees.elsevier.com.jmb

The Crystal Structures of Eukaryotic Phosphofructokinases from Baker's Yeast and Rabbit Skeletal Muscle

Katarzyna Banaszak[1], Ingrid Mechin[2], Galina Obmolova[2], Michael Oldham[3], Simon H. Chang[3], Teresa Ruiz[4], Michael Radermacher[4], Gerhard Kopperschläger[5] and Wojciech Rypniewski[1]*

[1]*Institute of Bioorganic Chemistry, Polish Academy of Sciences, Noskowskiego 12/14, 61-704 Poznan, Poland*
[2]*European Molecular Biology Laboratory, Hamburg Outstation, Notkestrasse 85, 22607 Hamburg, Germany*
[3]*Department of Biological Sciences, Louisiana State University, Baton Rouge, LA 70803, USA*
[4]*Department of Molecular Physiology and Biophysics, University of Vermont, 149 Beaumont Avenue, Burlington, VT 05405, USA*
[5]*Institut für Biochemie, Medizinische Fakultät, Universität Leipzig, Johannisallee 30, D-04103 Leipzig, Germany*

Received 11 October 2010; received in revised form 7 January 2011; accepted 9 January 2011
Available online 15 January 2011

Edited by M. Guss

Keywords:
glycolysis;
protein structure;
fructose 2,6-bisphosphate;
metabolism;
crystallography

Phosphofructokinase 1 (PFK) is a multisubunit allosteric enzyme that catalyzes the principal regulatory step in glycolysis—the phosphorylation of fructose 6-phosphate to fructose 1,6-bisphosphate by ATP. The activity of eukaryotic PFK is modulated by a number of effectors in response to the cell's needs for energy and building blocks for biosynthesis. The crystal structures of eukaryotic PFKs—from *Saccharomyces cerevisiae* and rabbit skeletal muscle—demonstrate how successive gene duplications and fusion are reflected in the protein structure and how they allowed the evolution of new functionalities. The basic framework inherited from prokaryotes is conserved, and additional levels of structural and functional complexity have evolved around it. Analysis of protein–ligand complexes has shown how PFK is activated by fructose 2,6-bisphosphate (a powerful PFK effector found only in eukaryotes) and reveals a novel nucleotide binding site. Crystallographic results have been used as the basis for structure-based effector design.

*Corresponding author. E-mail address: wojtekr@ibch.poznan.pl.

Present addresses: I. Mechin, Chemical and Analytical Sciences, Sanofi-Aventis, Mailstop N-103A, Route 202-206, Bridgewater, NJ 08807, USA; G. Obmolova, Johnson & Johnson, 1 Johnson & Johnson Plz, New Brunswick, NJ 08933-0001, USA; M. Oldham, Department of Biological Sciences, Purdue University, 915 West State Street, West Lafayette, IN 47904-2054, USA.

Abbreviations used: PFK, phosphofructokinase 1; Fru6-P, fructose 6-phosphate; Fru2,6-P_2, fructose 2,6-bisphosphate; *Sc*PFK, *Saccharomyces cerevisiae* PFK; RMPFK, rabbit muscle PFK; EM, electron microscopy; AS, ammonium sulfate; PEG, polyethylene glycol; MR, molecular replacement; PDB, Protein Data Bank.

Introduction

Glycolysis is the basis of both anaerobic respiration and aerobic respiration, and it occurs in nearly all organisms.[1] Phosphofructokinase 1 (PFK; EC 2.7.1.11) catalyzes the ATP-dependent phosphorylation of fructose 6-phosphate (Fru6-P) to form fructose 1,6-bisphosphate and ADP, and is a key element of control in the glycolytic pathway. PFKs are regulated by a number of effectors. In general, PFK is sensitive to the "energy level" of the cell, as indicated by the abundance of ATP relative to the products of ATP hydrolysis, but the mechanisms of control differ between eukaryotes and prokaryotes.[2] In a classic case of feedback inhibition, PFKs are inhibited by citrate, allowing feedback from the citric acid cycle.[3] In eukaryotes, but not in prokaryotes, PFKs are activated by fructose 2,6-bisphosphate (Fru2,6-P_2). This potent allosteric regulator is an additional means of controlling the rate of glycolysis, overriding inhibition by ATP, and making PFK in higher organisms sensitive to the action of the hormones glucagon and insulin.[4,5]

The intricacy of the control mechanism of PFK in eukaryotes is matched by its complex evolutionary history. In mammals, PFK subunits (~80 kDa) contain two clear sequence repeats, each homologous to a bacterial PFK subunit.[6] Three related types of mammalian PFK subunits combine in tissue-specific proportions into oligomers, among which the smallest active form is a tetramer, although the protein has also been observed in dimeric, octameric, or filamentous forms.[7–9] It interacts with proteins of the cytoskeleton.[10,11] By contrast, *Saccharomyces cerevisiae* PFK (*Sc*PFK) forms stable heterooctamers $\alpha_4\beta_4$ with a molecular mass of ~800 kDa and a sedimentation coefficient 21S.[12,13] Both α and β subunits are homologous to each other and show an internal sequence duplication similar to that seen in mammalian PFKs.[14] It has been proposed that gene duplications lead to a functional diversification of the multiplied catalytic and effector sites, allowing eukaryotes to develop their relatively more complex control apparatus for glycolytic processes.[6,15]

Crystallographic studies that reveal details of the enzymatic reaction mechanism and allosteric control have been carried out on bacterial PFKs.[16–20] Structural studies of eukaryotic PFKs lagged behind. Although crystals of rabbit muscle PFK (RMPFK) had been obtained as early as 1966,[21] they were unsuitable for crystallographic analysis. Both *Sc*PFK and RMPFK have been studied by electron microscopy (EM). The mammalian PFK was observed in various states of aggregation, while *Sc*PFK proved suitable for single-particle EM reconstruction, revealing a relatively detailed (10.8 Å) structure of the octamer.[22–24] The crystal structure of the first eukaryotic PFK, from *Trypanosoma brucei*, displays features in common with both ATP-dependent and pyrophosphate-dependent bacterial PFKs but does not show gene duplication typical of eukaryotes.[25] A recent article describes the crystal structure of PFK from *Pichia pastoris*.[26]

The first useful crystals of *Sc*PFK in the 12S form[27] were obtained as part of this study. The 12S form is a product of the limited proteolysis of native *Sc*PFK by α-chymotrypsin in the presence of ATP. Under these conditions, 21S octamers dissociate into 12S tetramers $\alpha_2''\beta_2'$, retaining catalytic activity and kinetic properties similar to those of the native enzyme.[28] We also obtained useful crystals of RMPFK with an 18-residue truncation at its C-terminus. This enzyme retains its allosteric behavior with respect to the substrate Fru6-P and is activated by Fru2,6-P_2, although its sensitivity to inhibition by ATP is reduced.[29]

Our study of the PFK crystal structure aimed to (i) examine the consequences of tandem gene duplication and fusion on protein structure; (ii) examine the relationship between these genetic events and the emergence of new elements in the enzyme's regulatory apparatus; and (iii) describe the structural bases of the enzyme's modulatory mechanisms that distinguish eukaryotic PFKs from their bacterial counterpart.

Table 1. Data collection and refinement statistics

	*Sc*PFK	RMPFK-lig	RMPFK-ATP
Data collection			
Space group	$P2_12_12_1$	$P6_122$	$P6_122$
Cell constants *a*, *b*, *c* (Å)	180.1, 186.2, 236.5	163.3, 163.3, 356.9	163.7, 163.7, 356.6
Resolution (Å)	35–2.9 (2.95–2.90)[a]	30–3.2 (3.26–3.20)	50–3.2 (3.26–3.20)
R_{sym}[b]	0.075 (0.557)	0.128 (0.778)	0.140 (0.879)
R_{meas}[c]	0.090 (0.803)	0.137 (0.719)	0.153 (0.753)
R^c_{pim}	0.041 (0.440)	0.048 (0.249)	0.046 (0.223)
$I/\sigma(I)$	15.1 (1.8)	16.8 (2.6)	17.8 (2.7)
Completeness (%)	98.5 (98.0)	100 (100)	99.9 (99.9)
Redundancy	4 (3)	8.3 (8.3)	11.2 (11.2)
Refinement			
Resolution (Å)	2.9	3.2	3.2
Number of reflections	172,763	47,108	47,363
R_{work}/R_{free}	0.25/0.31	0.23/0.30	0.24/0.30
Number of atoms			
Protein	44,310	11,408	11,404
Ligand/ion	288	192	208
Water	0	0	0
Average *B*-factor (Å^2)			
Protein	66.7	65.5	69.5
Ligand/ion	62.9	66.8	69.7
RMSD			
Bond lengths (Å)	0.011	0.016	0.013
Bond angles (°)	1.62	2.06	1.83

[a] One crystal was used for each data set. Values in parentheses are for the highest-resolution shell.
[b] Calculated by SCALEPACK.[30]
[c] Calculated by SCALA.[31]

Results

The structure of *Sc*PFK

The model of the 12S *Sc*PFK structure solved to 2.9 Å resolution (Table 1) consists of 6068 amino acid residues (97% of the crystallized protein) in eight polypeptide chains. Eight molecules of Fru6-P and eight molecules of Fru2,6-P_2 are bound to the enzyme. Although the protein used for crystallization was the tetrameric proteolytically cleaved 12S form[28] $\alpha_2''\beta_2'$, the two tetramers in the asymmetric unit form an octameric assembly resembling the native 21S *Sc*PFK octamer[23] $\alpha_4\beta_4$ (Fig. 1a). The proteolyzed subunits α'' and β' lack ~200 residues in the N-terminal regions found only in fungal PFKs. The α'' subunits are also cut near the C-terminus; however, in the crystal structure, the cleaved 60 residues remain associated with the bulk of the protein subunit. Therefore, the α'' subunit with the unexpected tail is named here α''^{+} (see Fig. S1, available online).

In the evolution of the complex structure of eukaryotic PFK, the basic building block resembling a bacterial PFK subunit has been conserved. The yeast PFK has 16 such elements embedded in its structure. Each α''^{+} subunit and β' subunit (Fig. 2a), as products of the duplication and fusion of ancestral genes, can be divided into two domains

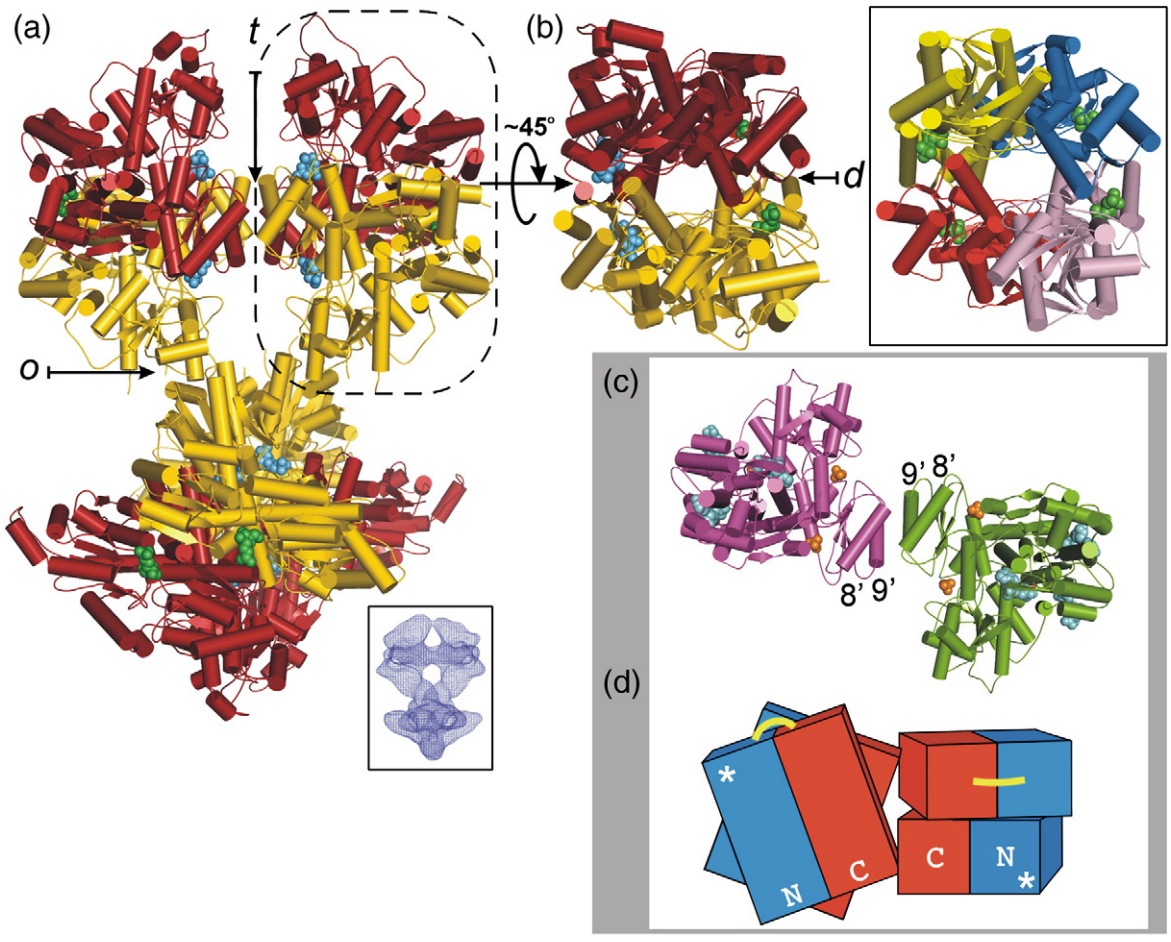

Fig. 1. The architecture of *Sc*PFK and RMPFK. (a) The structure of the *Sc*PFK octamer (size, 200 Å × 145 Å × 145 Å). The α''^{+} subunits are shown in yellow, and the β' subunits are shown in red. Fru6-P molecules are shown as green spheres, and Fru2,6-P_2 molecules are shown as blue spheres. The tetramerization ("t") and octamerization ("o") interfaces are indicated. The small inset shows the corresponding EM envelope of the native 21S *Sc*PFK particle.[23] (b) A different orientation of the $\alpha''^{+}\beta'$ dimer outlined in (a). The dimerization ("d") interface is indicated. A tetramer of *E. coli* PFK is shown on the right (PDB code 1PFK). (c) A pair of RMPFK subunits from the crystal structure. Helices forming the tetramerization interface are indicated. The subunits are in the same orientation as the two corresponding subunits in the top half of the *Sc*PFK octamer in (a). (d) A proposed scheme of an RMPFK tetramer. The RMPFK crystal structure is represented by the subunits marked by *. The N-domain (blue) and the C-domain (red), as well as the interdomain linkers (yellow), are indicated. The orientation of the dimer on the right is similar to that of the *Sc*PFK dimer in (b).

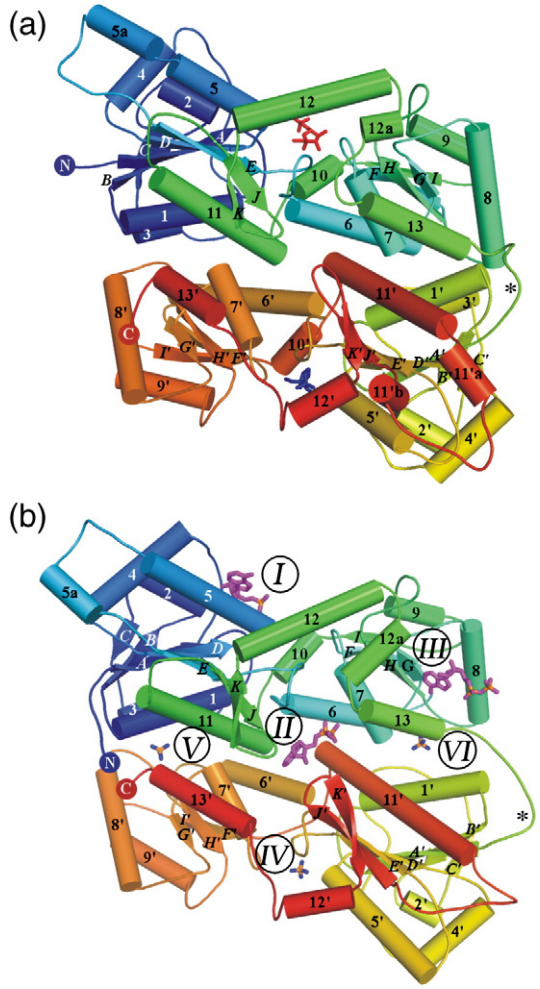

Fig. 2. The secondary structure elements of *Sc*PFK and RMPFK subunits. (a) The β subunit of *Sc*PFK. The secondary structure elements are labeled following the convention used in *E. coli* PFK (cf. Fig. 7c[18]). The interdomain 14-residue linker (marked with ∗) between the N-terminal domain and the C-terminal domain connects the α-helix 13 in the smaller subdomain of the N-terminal half with the β-strand A′ from the larger subdomain in the C-terminal half. Fru6-P substrate is shown as red sticks, and Fru2,6-P_2 effector is shown as blue sticks. (b) A similar view of the RMPFK subunit with ligands (sticks): ADP in the active site (I), in the subunit center (II), and in the smaller subdomain of the N-terminal half (III). Three bound phosphate/sulfate ions are also shown: in the 2-phosphate cavity of the Fru2,6-P_2 effector site (IV) and in cavities corresponding to prokaryotic effector sites (V and VI).

(N-terminal and C-terminal halves), each resembling the prokaryotic PFK subunit (Fig. S2). Each domain consists of two subdomains of different sizes, with each subdomain having an αβα-sandwich fold.

Also, the mutual arrangement of bacterial PFK subunits has been conserved in the *Sc*PFK structure, similarly to the PFK structure of *P. pastoris*,[26] in that each of its four αβ dimers resembles a bacterial PFK tetramer (Fig. 1a and b). The interactions between α subunits and β subunits determine the location of the active and effector sites in the eukaryotic enzyme. Dimerization interface is formed when the N-terminal domain of the α''^{+} subunit interacts with the N-terminal domain of the β′ subunit and when their C-terminal domains also interact. A tetrameric 12S particle is formed when a pair of $\alpha''^{+}\beta'$ dimers associates in such a way that the α''^{+} subunits contact the β′ subunits of the other dimer. Tetramerization interactions involve corresponding secondary structure elements of the α''^{+} and β′ subunits (helices 8′ and 9′ from each subunit), but the interacting residues differ between the two types of subunits. The corresponding contacts in RMPFK are symmetric. Two 12S tetramers associate through the interactions between α''^{+} subunits from neighboring tetramers. Consequently, four α''^{+} subunits form the core of the heterooctamer, while four β′ subunits are packed on the outside (Fig. 1a). Octamerization interface is made by interactions within two pairs of α''^{+} subunits and involves helices 4′ and 5′ from each α''^{+} subunit and probably some residues from the segment 894–919 that are disordered in the crystal due to cleavage by α-chymotrypsin. The tetramers are rotated 75° to each other, similar to the cryo-EM 21S PFK reconstruction.[24] The association of the tetrameric 12S *Sc*PFK particles into native-like octamers is an interesting example of a protein resembling the native structure better in the crystal than in solution. This is probably due to the high concentration of protein in the crystallization solution.

Is the enzyme in active form?

The *Sc*PFK structure is likely to represent the active state, as indicated by the alignment of protein subunits, the binding between them the substrate Fru6-P and the activator Fru2,6-P_2, and a comparison with EM studies. The overall structure is closely similar to the EM reconstruction of *Sc*PFK obtained in the presence of Fru6-P, where the relative orientation between the two halves of *Sc*PFK is 75°, as opposed to the 46° observed for the enzyme in the presence of inhibitory amounts of ATP.[24]

The alignment of subunits within the *Sc*PFK αβ dimers resembles the bacterial PFK tetramers described as the active R-state. First, the α''^{+} and β′ subunits are 4.6–5.0 Å, indicating a layer of water molecules typical of the R-state of the bacterial PFKs and different from the bacterial T-state where the residues interact directly.[20] Moreover, the conformation of the crucial basic residue in the Fru6-P binding pocket of *Sc*PFK (Arg391 in α''^{+} and Arg383 in β′) is the same as in the bacterial PFK R-state (Table S1). In the T-state *E. coli* PFK, this residue is rearranged and no longer points towards the

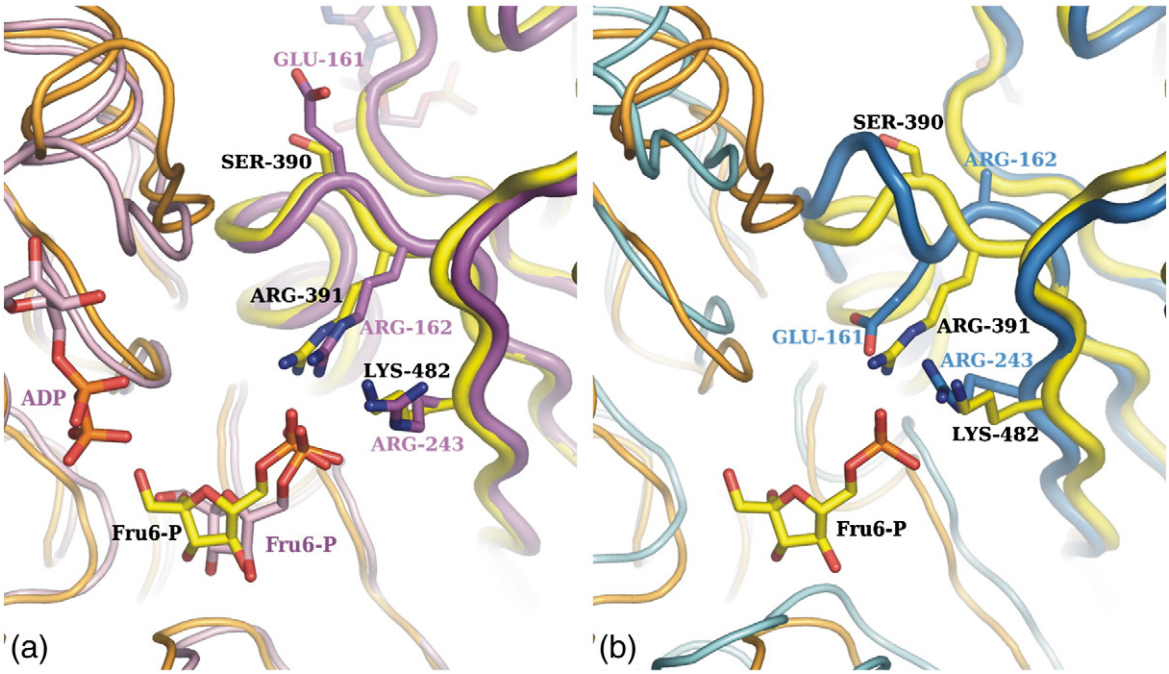

Fig. 3. Comparison of *Sc*PFK with the R-state and the T-state of bacterial PFK. (a) The superimposition of *E. coli* PFK structure in the R-state (violet; PDB code 4pfk) on *Sc*PFK. (b) The superimposition of the T-state of bacterial PFK (blue; PDB code 6pfk) on the *Sc*PFK structure. In *Sc*PFK (yellow and orange; labeled black), the conformation of the loop containing Arg391 (crucial for binding the sugar ligands) corresponds to the R-state. Neighboring subunits can be distinguished by the different thicknesses of the "tubes" representing the main chains.

binding pocket (Fig. 3). By analogy to bacterial PFK, one would expect a similar rearrangement of Arg residues in the *Sc*PFK T-state.

The binding of Fru6-P and Fru2,6-P_2

In the course of evolution, gene duplication and subsequent mutations led to the emergence of new regulatory mechanisms controlled by new effectors. The N-terminal domain of the eukaryotic PFK subunit has retained the catalytic role, while the C-terminal half has acquired a regulatory function (Fig. 2a).

The active sites

Subunits α and β each possess a catalytic site located on one side of the αβ dimer, where the N-terminal halves interact (Fig. 4a). Each β-D-Fru6-P is bound between the two subdomains of the N-terminal half of one subunit, and, simultaneously, the ligand's 6-phosphate group interacts with two basic side chains of the neighboring subunit (Fig. 4c, e, and g). Four pairs of such sites are located on the outer surface of the *Sc*PFK octamer (Fig. 1a).

The N-terminal domains also contain ATP substrate binding cavities. These binding pockets are in the larger subdomains (near the Fru6-P sites) and are unoccupied in the *Sc*PFK crystal structure (the crystals were intolerant to soaking), but correspond closely to the ATP binding sites in RMPFK and prokaryotic PFKs (Fig. 4c).

The *Sc*PFK active sites resemble those of the bacterial PFKs in the R-state. The residues that have been identified in bacterial PFKs as important in enzymatic activity are conserved in the *Sc*PFK structure in terms of their chemical identity and three-dimensional structure (Table S1). It is reasonable to conclude that the reaction mechanism is also conserved.

The Fru2,6-P_2 effector site

The activator's β-D-Fru2,6-P_2 electron density map could be clearly recognized in the C-terminal domains of α''^{+} and β′ subunits, and the principle of enzyme activation by Fru2,6-P_2 can be deduced from the crystal structure. A pair of activator sites is located on the side opposite to the pair of active sites on each *Sc*PFK $\alpha''^{+}\beta'$ dimer (Fig. 4b). The eight effector sites lie on the inner surface of the *Sc*PFK octamer. Each Fru2,6-P_2 molecule binds at the intersubunit interface in a cavity between the subdomains of the C-terminal domain of one subunit, while the ligand's 6-phosphate group extends across the dimerization interface and interacts with two basic amino acid side chains of

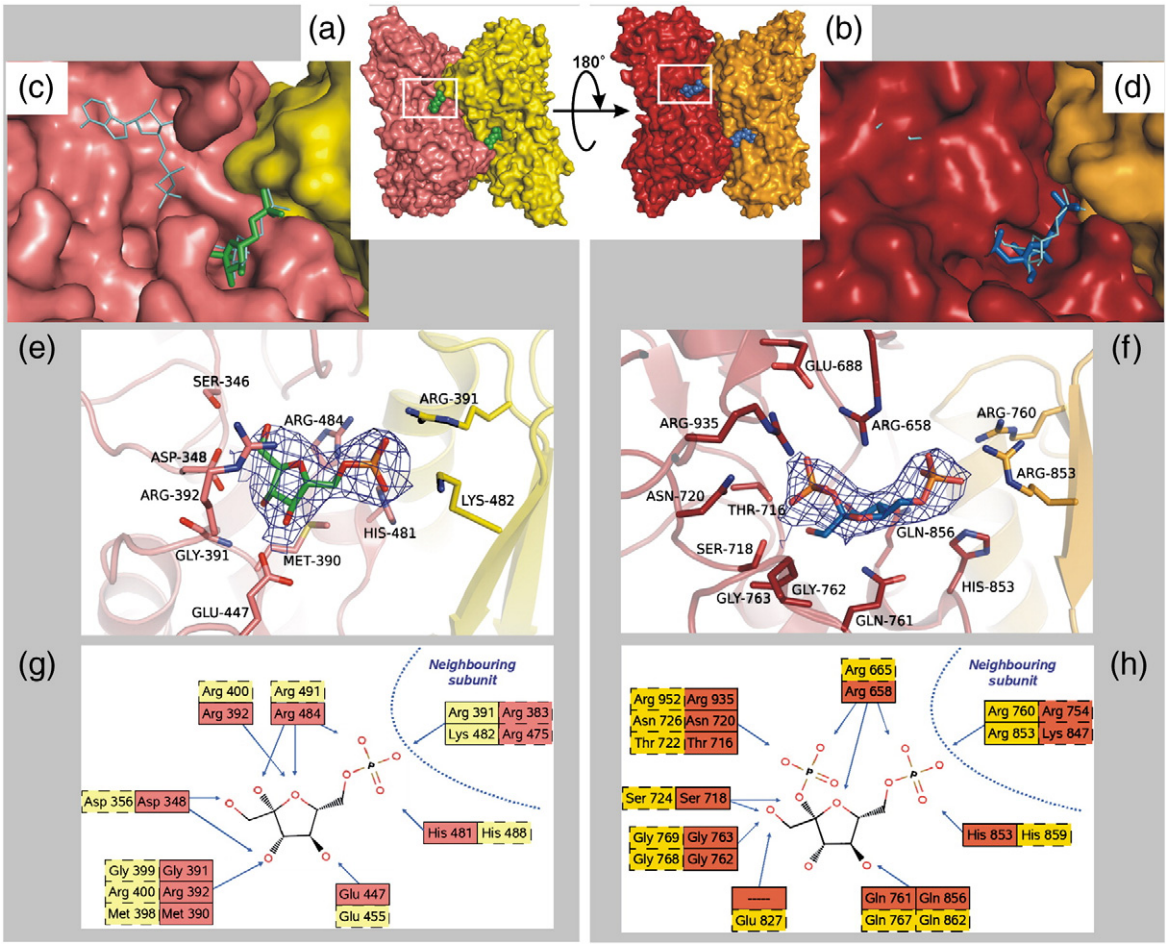

Fig. 4. Ligands binding to *Sc*PFK. (a) A pair of Fru6-P substrate molecules (green) bound to the N-terminal halves of α''^{+} (yellow) and β' (salmon) *Sc*PFK subunits. (b) A pair of Fru2,6-P_2 molecules (blue) bound at the C-terminal halves of α''^{+} (orange) and β' (red) subunits. (c and d) Details of the areas boxed in (a) and (b). Superimposed are fructose 1,6-bisphosphate and ADP (cyan) modeled in comparison with *E. coli* PFK (PDB code 1PFK). Note the loss of the nucleotide binding cavity near the Fru2,6-P_2 site in (d). (e) Details of Fru6-P binding and (f) Fru2,6-P_2 binding. The omit electron density map is contoured at the 3σ level. (g) The scheme of protein–Fru6-P interactions with α (yellow) and β (salmon) *Sc*PFK subunits (labels outlined in broken lines are for the second site shown in (a)). (h) A similar scheme for the Fru2,6-P_2 binding sites.

the C-terminal domain of the neighboring subunit (Fig. 4d, f, and h). It is clear from the analogy with Fru6-P binding that the activator cavity evolved from the sugar substrate binding pocket of the duplicated active site following ancestral gene duplication and fusion. A comparison of the Fru6-P and Fru2,6-P_2 binding sites reveals features that are common and some that differ, reflecting different ligand binding specificities (Table S1). O5, which closes the sugar ring, is always associated with an Arg residue. O4 interacts with a Glu or a Gln. 6-Phosphate is coordinated by a His and an Arg of one subunit, and by two Arg residues or an Arg and a Lys from another subunit (Fig. 4e–h). Differences appear around positions 1, 2, and 3 of the sugar rings. A characteristic feature of the Fru2,6-P_2 binding pocket is an interaction with Arg residue (Arg952 in α''^{+} and Arg935 in β') coming from a new element of the secondary structure: a loop of nine amino acid residues located between helices 12′ and 13′ (Figs. S1 and S2). This residue, together with Arg665 and Glu694 in α''^{+} (or Arg658 and Glu688 in β'), forms a motif for binding the activator's 2-phosphate (Fig. 4f). The two Arg residues coordinate the phosphate group, while the Glu is between the Arg side chains and stabilizes them with H-bonds. A similar motif is found in RMPFK.

The activation effect of Fru2,6-P_2 results from its simultaneous binding to both C-terminal halves of two neighboring subunits, thus stabilizing the whole dimer in the active conformation, including the N-terminal domains with their active sites. Specific protein–ligand interactions take place predominantly around the two phosphate groups and

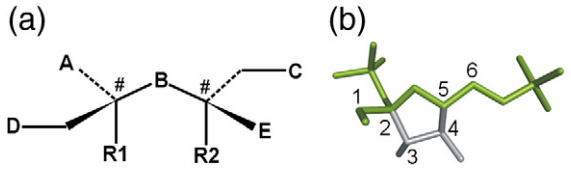

Fig. 5. Pharmacophore of an activator of eukaryotic PFK. (a) A and C are phosphate, sulfate, or sulfonate groups; B is an ether or thioether group; D is a phosphate, sulfate, sulfonate, or hydroxyl group; E is a hydrogen atom; # is a carbon atom with an sp^3 hybridization; and R1 and R2 stand for a hydrogen atom or –CXH-OH or CX=O groups (where X is a hydrogen atom or a bond to the other R via a $–CH_2–$ group). A pharmacophore of an inhibitor is similar, except that it lacks the bridging group (i.e., C is a hydrogen atom). Such a ligand should bind unproductively, blocking the binding site against the natural activator and thus stabilizing the inactive T-state. (b) The green part of the Fru2,6-P_2 effector was the basis of the pharmacophore design. It forms most of the interactions with the protein. We acknowledge the works of Kelley *et al.*[32] and Ishikawa *et al.*,[33] who probed the Fru2,6-P_2 activator site with several analogues of Fru2,6-P_2.

the ether group, while the C3–C4 edge of the ribose ring makes fewer contacts. We have used the key features of Fru2,6-P_2 interactions in the effector site to design pharmacophores of an activator and an inhibitor of eukaryotic PFKs (Fig. 5) (international patent application numbers PCT/PL2008/000087 and PCT/PL2008/00008831).

The area near the Fru2,6-P_2 binding pocket that corresponds to the nucleotide binding part of the ancestral active site has not retained any recognizable feature of a binding cavity (Fig. 4d), with the space being completely filled by protein atoms, similarly to the PFK structure of *P. pastoris*.[26] This puts to rest the speculation that this area has evolved into the ATP inhibitor binding site. The related RMPFK structure demonstrates this even more clearly because no nucleotide is found in this location even when ATP and ADP bind elsewhere in the protein.

The structure of RMPFK

Two structures of RMPFK, with 18 amino acid residues truncated at its C-terminus, have been analyzed at 3.2 Å resolution: one of the protein crystals was soaked in a mixture of Fru6-P, Fru2,6-P_2, and ADP (named RMPFK-lig), and another was soaked in ATP (RMPFK-ATP) (Table 1). Each crystal structure contains two RMPFK subunits per asymmetric unit; each chain of 748 amino acid residues interacts with six ligands interpreted as either ADP, ATP, or phosphate ions.

The fold of the RMPFK subunit resembles the *Sc*PFK subunit (Fig. 2b) or a pair of bacterial PFK subunits.[20] The RMPFK subunits do not aggregate in the crystal lattice into active oligomers, which in the case of mammals are at least tetramers. The RMPFK crystal structure consists of one half of such a tetrameric assembly: a pair of subunits, one from each dimer, connected by the tetramerization interface (Fig. 1c). The RMPFK subunits do not form dimerization contacts—which have been observed in *Sc*PFK to be essential for the catalytic activity and allosteric behavior of the enzyme—coming out of Fru6-P and Fru2,6-P_2 binding at this interface. The reason that such dimerization interactions are not observed in the RMPFK crystal is probably the low pH of crystallization. pH-dependent reversible dissociation and inactivation of RMPFK have been observed and proposed to result from a protonation of His residues.[34,35] Three possibilities can be proposed based on the crystal structure: His199, His298, and His661. The equivalents of His199 in the *Sc*PFK structure (His389 in the α subunit; His381 in the β subunit) interact across the intersubunit interface with two conserved Gly residues (residues 205 and 206 in β; residues 214 and 215 in α), which in the rabbit enzyme correspond to Gly24 and Gly25. Protonation of this His is therefore likely to affect the intersubunit interface. The other two His residues lie in sugar binding cavities: His298 in the active site, and His661 in the Fru2,6-P_2 effector site. In the *Sc*PFK structure, the equivalent residues (His488 in α, His481 in β; His859 in α, His853 in β) each interact with the 6-phosphate of the sugar. When protonated, they are likely to interfere with the binding of the sugar ligands and to counteract the stabilizing and activating effects of the ligands on the enzyme.

However, the two RMPFK subunits in the asymmetric unit form the tetramerization interaction known from the *Sc*PFK structure to hold together pairs of αβ dimers. The contacts in RMPFK are predominantly hydrophobic and based on different amino acid sequences compared to the contacts in *Sc*PFK, yet involve elements of the secondary structure equivalent to those in *Sc*PFK (α-helices 8′ and 9′ from each RMPFK chain) and hold the subunits in the same relative orientation (Fig. 1c). The difference from the heterooctameric *Sc*PFK is that the interactions in the homooligomeric RMPFK are symmetric.

The observation that the subunit fold and the tetramerization interface of RMPFK are conserved in comparison with *Sc*PFK strongly suggests that the dimerization interaction, although unobserved in the RMPFK crystal structure, occurs under physiological pH and is constructed in a manner known from the *Sc*PFK structure, where the N-terminal and C-terminal halves of subunits interact N-to-N and C-to-C. Earlier mutagenesis studies also can be interpreted in[36,37]—or can directly support[38]—such a manner of dimerization. The above indicates

that a tetramer of the mammalian protein resembles a tetramer of *Sc*PFK. A model of an RMPFK tetramer (Fig. 1d) can easily be constructed by "associating" with each of the two RMPFK subunits in the asymmetric unit the missing chain at the dimerization interface, using the αβ dimer of *Sc*PFK as guide. The resulting tetramer has a structure very similar to that of the 12S *Sc*PFK particle; in other words, it consists of two dimers, each resembling a bacterial PFK tetramer.

The binding of ADP, ATP, and phosphate/sulfate ions

Three nucleotides are bound to each RMPFK subunit: one at the active site in the nucleotide binding cavity, another in the center of the subunit (at a site not described before), and a third in the smaller subdomain of the N-terminal half, in a pocket similar to the ATP binding site found in the β-chain of *P. pastoris* PFK.[26]

In the active sites, there are ADP molecules in RMPFK-lig and ATP molecules in RMPFK-ATP. The binding interactions are similar to those found in bacterial PFK,[18] with full conservation of interacting amino acid residues (Table S1).

A novel nucleotide binding cavity is observed in the center of each RMPFK subunit, in a pocket between the N-terminal domain and the C-terminal domain, under two characteristic β-hairpins (strands J,K and J′,K′). Electron density was interpreted as an ADP molecule in both RMPFK-lig and RMPFK-ATP structures (Fig. 6), indicating that soaking crystals in ATP did not displace the ADP that was lodged there during crystallization. The ADP molecule is buried inside the protein, and its numerous interactions indicate a well-tailored binding site. The adenine ring of the ligand makes stacking interactions with Phe308 and Phe671, while its *exo*-amine group is at hydrogen-bonding distance from Asp543. The hydroxyl groups of the ribose ring interact with the main-chain amine group of Asn341 and possibly with the side chain of Met713. The phosphate groups interact at hydrogen-bonding distances with the hydroxyl groups of Tyr214 and Ser377, the amine group of the Lys678 side chain, and the amide group of Asn381. The central part of the eukaryotic subunit has not been identified as a binding site before. Although its function is unknown, the mutation of Asp543 to Ala—associated with Tarui disease[39] (Fig. S4), which would remove the H-bond with the adenine—suggests that the binding of ADP at this site has a functional role. The binding cavity in the center of the subunit invites speculation that the nucleotide modulates the relative movement of the PFK subdomains described earlier for bacterial PFK, bringing substrates together and positioning them for phosphoryl transfer.[20] This ADP lodged between the domains could possibly be an activator signaling a "low-energy level" in the cell.

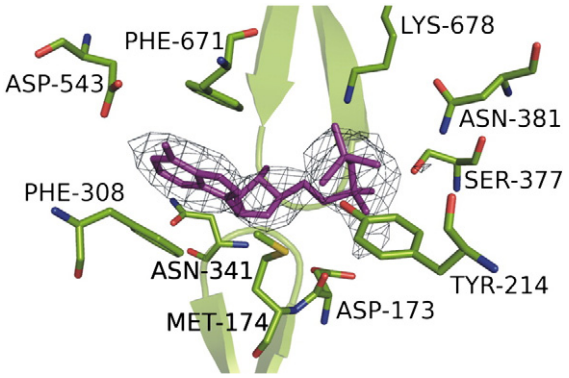

Fig. 6. ADP binding in the RMPFK subunit center. The omit electron density map is contoured at the 3σ level.

The third nucleotide molecule binds between helices 8 and 13 in the N-terminal domain of the RMPFK subunit. In RMPFK-lig, the density has been interpreted as ADP; in RMPFK-ATP, the density has been interpreted as ATP (Fig. 7). The adenine moiety and the ribose ring fit into a well-defined cavity, while the phosphate groups protrude, suggesting that the site does not discriminate between the two nucleotides. The specificity of this site is therefore unclear. In both RMPFK structures, the orientation of the bound nucleotides differs by 180° from the ligand found in the corresponding ATP binding site in *P. pastoris* PFK,[26] with the phosphate groups pointing in the opposite direction (Fig. 7). In the RMPFK structures, the adenine rings stack on one side against Trp227 and on the other side along the aliphatic part of the Lys386 side chain. The *exo*-amine group of the adenine interacts with the hydroxyl group of Tyr385, its N1 interacts with the amine group of Val228, and its N6 interacts with the side chain of Arg246. The ribose ring forms interactions with Lys386 and His242, while the phosphate groups in the case of RMPFK-ATP interact with the side chains of His242, Arg246, and His390, and with the amine group of Ile391. In the case of bound ADP (RMPFK-lig), the phosphate groups do not appear to make hydrogen-bonding interactions with the protein.

Neither Fru6-P nor Fru2,6-P_2 was bound to RMPFK despite their presence in the crystallization medium. The probable reason is the lack of dimerization interface between subunits in the low pH of crystallization. However, the electron density of a sulfate or phosphate ion was observed in the activator site at a location corresponding to the 2-phosphate of Fru2,6-P_2 in *Sc*PFK (Fig. S3).

More ligands are observed in cavities corresponding to the effector sites of prokaryotic PFK. In bacteria, the single effector site (per subunit) is able to bind

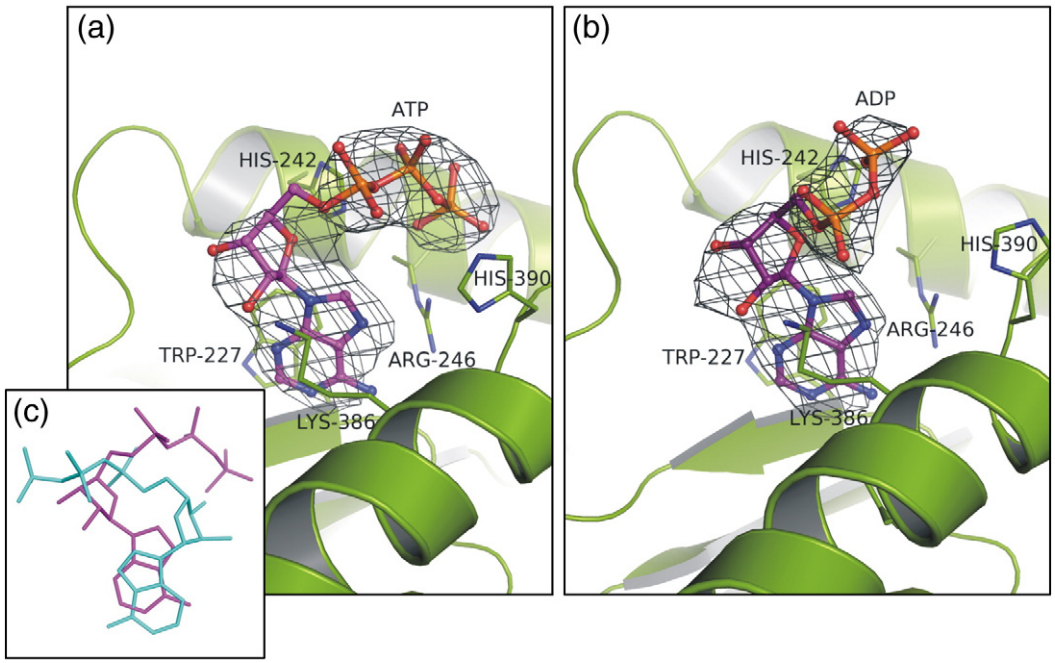

Fig. 7. The nucleotide binding site in the smaller subdomain of the N-terminal half of the RMPFK subunit. (a) ATP molecule in the RMPFK-ATP structure. (b) ADP molecule in the RMPFK-lig structure. The omit electron density maps are contoured at the 3σ level. (c) Superposition of the ATP molecules from RMPFK-ATP (violet) and PpPFK[26] (cyan).

either activator or inhibitor molecules, and a pair of effector sites from two neighboring subunits is localized at the same intersubunit interface. In the double-sized eukaryotic subunits, these regions are no longer symmetric, and they now belong to one subunit. Nevertheless, the cavities have been maintained throughout evolution (they are also observed in *Sc*PFK), have a size similar to that of the bacterial effector site, and have retained their basic character to some extent. The cavities—one near the loop linking the two domains of the RMPFK subunit, and the other near the N-terminus and the C-terminus (Fig. S5)—are occupied by phosphate or sulfate ions at positions corresponding to the terminal phosphate of ADP when compared with *E. coli* PFK.[18] The possible function of the two sites was assigned on the basis of previous mutagenesis studies. According to these studies, the mutation of Arg to Leu abolished the enzyme's inhibition by citrate in rabbit PFK-C.[15] This corresponds to Arg39 in RMPFK interacting with the phosphate/sulfate ion near the amino acid chain termini. In another mutagenesis study, replacing two Arg residues in mouse PFK by Ala was found to reduce or abolish inhibition by ATP.[40] These residues correspond to Arg420 and Arg424 in the RMPFK structure, and they interact with the ion in the cavity close to the interdomain linker. Moreover, two of the known mutations in human PFK—Arg39Pro/Leu[39] (Fig. S4)—are associated with the Tarui disease map in the location near the terminal ends in RMPFK, attesting to this site's physiological relevance.

Discussion

The crystal structure of *Sc*PFK demonstrates how gene duplication and subsequent evolution modify structure and regulatory functions. The basic fold of the ancestral prokaryotic PFK has been preserved to a remarkably high degree (down to the details of the secondary structure) despite the doubling of subunit size, evolving new functionalities and additional levels of oligomerization. The structural elements that are common to *Sc*PFK and RMPFK and are absent in bacterial enzymes point to the new functionalities characteristic of eukaryotes, such as the loop that binds Fru2,6-P_2 (marked "4" in Fig. S2) or bulges "1" and "2" of unknown functions, which are possibly involved in intermolecular interactions (e.g., with the cytoskeleton).[10] One can also see how *Sc*PFK forms stable octamers while the mammalian PFKs oligomerize variously. The ability of *Sc*PFK to form "closed" octamers follows from (i) the existence of two types of subunits, and (ii) the fact that α subunits interact only with β subunits (and *vice versa*) at the dimeric and tetrameric levels. These two conditions guarantee that an *Sc*PFK tetramer has two distinct faces. On one side, the two α subunits are free to interact with a similar face of another

tetramer to form a native octamer (Fig. 1a). On the other side of the tetramer, the β subunits form a "dead end" that is unable to participate in further aggregation. By contrast, a tetramer of similar topology but consisting of only one type of subunit (homotetramer), like the mammalian PFK, always presents two similar faces. Consequently, if one side can interact further, so can the other. Based on the crystallographic model of RMPFK, one can examine possible paths of further oligomerization of the enzyme (Fig. S6), as indicated by previous EM and sedimentation studies where the protein was observed in various states of oligomerization: dimers, tetramers, octamers, and higher assemblies up to filamentous structures.[41] The two possible areas of interaction between RMPFK tetramers are indicated: (i) contacts involving helices 4′ and 5′, analogous to the octamerization interaction between the α subunits in *Sc*PFK (in the case of the mammalian enzyme, two identical faces would exist on opposite sides of the RMPFK tetramer); and (ii) interactions involving helices 8 and 9 of the N-domain, which correspond to helices 8′ and 9′ of the C-domain, where they are responsible for tetramer formation. Sequence analysis indicates, however, that the external surface of the two helices in the N-domain is highly hydrophilic, consisting largely of Arg and Gln residues, as opposed to the hydrophobic residues in helices 8′ and 9′ that form the tetramerization interface. Structure-based site-directed mutagenesis studies, combined with EM, could be used to resolve whether one of these alternatives is physiologically relevant.

The *Sc*PFK structure shows details of Fru6-P interactions in the active site and the topology of the binding pocket of the second substrate, ATP. The binding of Fru2,6-P_2 to the C-terminal half of each subunit reveals the principle of action of this most powerful activator of eukaryotic PFKs. The crystal structures presented also show that the duplicated ATP substrate binding site did not become the new ATP inhibitor site. This binding pocket in the C-terminal domain has been lost in the course of evolution.

The nucleotide binding study of the RMPFK structure revealed a novel binding pocket that could be the ADP activator binding site. The other nucleotide binding site has been proposed by Sträter *et al.* as the ATP inhibitor site in *P. pastoris* PFK.[26] One needs to note, however, the puzzling difference in the mode of binding of the nucleotides at this site between the fungal enzymes and the mammalian enzymes.

The ions found in the RMPFK structure demonstrate that binding pockets in locations corresponding to the effector sites of bacterial PFK are still present in the eukaryotic enzyme, although their function is unclear.

An important area of medical research is aimed at anti-fungal therapies. Pathogenic fungi are difficult targets because, being eukaryotes (like the organisms they infect), they are harder to discriminate against than bacteria. The PFK structural features that distinguish fungi from other eukaryotes (e.g., the elements responsible for their distinct oligomerization) can be mapped on the *Sc*PFK structure and used as drug targets. On the other hand, the known mutations responsible for PFK-based metabolic disorders can be mapped on the structure of RMPFK and used similarly (Fig. S4).

Fru2,6-P_2 is a key element of metabolic control in eukaryotes; therefore, understanding the detailed mechanism of Fru2,6-P_2 activation opens possibilities for a rational design of metabolic modulators with potential applications in industry and medicine. Firstly, this effector site promises to be a particularly good target because Fru2,6-P_2 is a very specific compound that is known to act on only two enzymes (PFK and the functionally opposite fructose-1,6-bisphosphatase); therefore, its binding site should be highly selective. Secondly, the binding of Fru2,6-P_2 is clear, and it is possible to define which of the ligand's features are essential (e.g., the unusually positioned 2-phosphate makes the ligand specific, while 6-phosphate makes it effective, acting as the grappling hook). Lastly, the elements of the binding cavity responsible for ligand binding are also well defined, offering good guidelines for structure-based design (Fig. 5).

The two structures of eukaryotic PFKs give a measure of the complexity and evolutionary history of PFK in eukaryotes, provide the three-dimensional structural framework for interpreting numerous biochemical and mutagenesis results obtained over the years, and will serve as a point of reference in future studies. They also offer a rare glimpse, in atomic detail, into the realm of unusually large protein structures whose complexity and fragility make them a hard target for detailed studies.

Materials and Methods

*Sc*PFK

*Preparation of 21S Sc*PFK

The source of PFK was the recombinant strain PS1 of *S. cerevisiae* (*MATa ura3–52 leu2–3,112 his4–519 pep4–3 gal2 cir*$^+$) that carries the *PFK1* and *PFK2* genes on a multicopy vector. PS1 is the cir$^+$ form of the strain described by Seeboth *et al.*[42] The enzyme was purified according to the method of Hofmann and Kopperschläger,[2] with the following modifications: (i) instead of sonication, yeast cells were disrupted by shaking for 5 min in the Vibrogen Cell Mill (type Vi 4; Bühler, Tübingen, Germany) in a buffer consisting of 50 mM sodium phosphate (pH 7.0), 5 mM β-mercaptoethanol, and 0.5 mM phenylmethylsulfonyl fluoride (buffer A); (ii) the first ammonium sulfate (AS) precipitation was replaced by fractional precipitation

with polyethylene glycol (PEG) 6000 at 3.5% and 14% (wt/vol) PEG (the first pellet was discarded, and the second pellet containing the enzyme was suspended in buffer A); and (iii) in the affinity chromatography step, via Cibacron Blue F3G-A Sephadex G 100, the enzyme was eluted using buffer A with the addition of 5 mM ATP and 10 mM $MgCl_2$ instead of AS.

Preparation and assay of 12S PFK

Limited proteolysis of the 21S PFK was carried out with α-chymotrypsin in accordance with Bär *et al.*, except that gel filtration was replaced by chromatography using an HPLC Resource Q column (twice).[43] The purified 12S PFK showed no microheterogeneity on SDS-PAGE. Enzyme activity was measured by mixing 1.0 mL of solution containing 100 mM imidazole/HCl (pH 7.2), 3 mM Fru6-P, 0.6 mM ATP, 1 mM AMP, 5 mM magnesium sulfate, 5 mM AS, 0.2 mM NADH, and coupling enzymes (glycerol-3-phosphate dehydrogenase, triosephosphate isomerase, and aldolase) with 20 μL of protein solution. NADH concentration at 25 °C was observed at 340 nm wavelength: the decrease of two molecules of NADH corresponds to the loss of one molecule of Fru6-P.

Crystallization

The 12S PFK was crystallized in accordance with Obmolova *et al.*[27] Before crystallization, the protein suspension was dialyzed at 4 °C against the 20 mM Hepes buffer (pH 7.4) containing 1 mM ethylenediaminetetraacetic acid, 0.2 M sodium acetate, 0.1 M AS, 2 mM dithiothreitol, 0.1 mM phenylmethylsulfonyl fluoride, and 10 mM Fru6-P. Fru2,6-P_2 was added to the protein solution to a concentration of approximately 5 mM. The crystals were grown by hanging-drop vapor diffusion at 4 °C with a reservoir solution containing 6–10% PEG 4000 and 0.2 mM sodium acetate in 0.1 M 4-morpholineethanesulfonic acid buffer (pH 6.0). The orthorhombic needles appeared within 2 weeks.

Data collection and processing

X-ray data were recorded on beamline BW7B of the European Molecular Biology Laboratory at the DORIS Storage Ring (DESY, Hamburg, Germany) under cryo-conditions at 100 K and at an X-ray wavelength of 1.1044 Å and processed with the HKL package.[30] The data collection statistics are summarized in Table 1.

Structure determination

The 12S PFK crystal structure was solved by molecular replacement (MR) aided by the results from the single-particle EM of the 21S PFK.[23] The use of the EM structure allowed us to reduce the number of possible MR solutions from, originally, 16 to only 2. In addition, the EM map showed that one bacterial tetramer corresponds to one αβ dimer in yeast. Therefore, the atomic coordinates of *E. coli* PFK R-state [Protein Data Bank (PDB) code 1pfk[18]] could be used as the starting model for MR. The asymmetric unit of the 12S PFK crystal was estimated to contain two 12S PFK tetramers. Initially, we identified two positions, which together resembled one half of the 21S particle established by EM. In the next stage of MR, the two bacterial PFK tetramers were used together as search model to identify the other half of the yeast structure. The solution was checked for consistency with the EM envelope and for self-rotation function. Calculations were carried out using the program AMoRe[44] from the CCP4 program suite.[45]

Electron density modification and model refinement

Density modification was carried out with DM[46] and included solvent flattening, histogram matching, and noncrystallographic symmetry averaging. Phases were extended in the course of DM from the range of 15–4 Å (used in MR) to the full extent of the experimental structure factor amplitudes of 35–2.9 Å. The model was refined using the program CNS[47] with noncrystallographic symmetry restraints and bulk solvent correction. Initially, only the overall *B*-factor was refined; however, in the course of the refinement, group *B*-factors were refined as well. The final model statistics were calculated using PROCHECK.[48]

Rmpfk

Construction, expression, and purification of recombinant RMPFK

Full-length cDNA encoding RMPFK[36] was mutated at position E763 (GAG to UAG) using a Promega site-specific mutagenesis kit. This mutation deleted 18 residues from the C-terminus of RMPFK. This truncated version of RMPFK cDNA was inserted between the NdeI site and the EcoRI site of the pET5a plasmid (Novagen) and transformed into a *pfk*-deficient *E. coli* host strain lysogenized with phage lambda DE3 carrying the T-7 phage RNA polymerase gene (DF_{1020}DE3). The transformed cells were grown in LB broth containing 100 μg/mL ampicillin until the midexponential phase. The target gene was induced by adding IPTG to 1 mM, and the culture was incubated at 30 °C overnight with slow shaking. Cell pellets were suspended in 50 mM Tris phosphate (pH 8.2) containing 0.1 mM ethylenediaminetetraacetic acid and 1 mM β-mercaptoethanol. The supernatant of the sonicated lysate was analyzed for PFK activity. The extracted recombinant RMPFK was purified to homogeneity by chromatography using Cibacron Blue 3GA (Sigma), diethylaminoethyl cellulose (DE-52; Whatman), and ATP-N^6-agarose (A9264; Sigma) columns. The purity of the RMPFK protein was verified by SDS-PAGE. The purified protein was precipitated to 60% by ultrapure AS (Fluka); redissolved to a concentration of 10–12 mg/mL in 50 mM 2-{[2-hydroxy-1,1-bis(hydroxymethyl)ethyl]amino}ethanesulfonic acid (pH 7.0), 10 mM dithiothreitol, and 10 mM ATP; and dialyzed against the same buffer.

Assay of RMPFK activity

PFK activity was assayed using a reaction coupled with NADH oxidation according to two protocols.[36] One protocol, at pH 8.2, was used for measuring the maximum PFK activity in fractions during the purification and determination of the K_m values of substrates for the truncated RMPFK. A second protocol, at pH 7.0, was used to determine the response of the truncated RMPFK protein to inhibitors and activators.

Preliminary crystallization and X-ray diffraction trials

The first successful crystallization trials were carried out at the High-Throughput Screening Laboratory of the Hauptman–Woodward Institute (Buffalo, NY) using the microbatch method.[49] Rod-shaped crystals were observed in 0.1 M $MgSO_4$, 0.1 M sodium acetate (pH 5.0), and 20% PEG 400. The crystallization conditions were further optimized using the hanging-drop method.

Crystallization, X-ray data collection, and processing

Crystals used for the final X-ray diffraction experiments were obtained in the presence of Fru6-P, Fru2,6-P_2, and ADP by hanging-drop vapor diffusion, with the reservoir solution containing 16% PEG 400, 0.1 M $MgSO_4$, and 0.1 M acetate buffer (pH 5.3). The crystals had the form of needles with a hexagonal cross section and appeared within a week. Prior to data collection, the crystals were transferred to a cryoprotectant solution containing the same salts as the reservoir solution and 30% vol/vol PEG 400 and protein ligands. The ligands were either a mixture of Fru6-P, Fru2,6-P_2, and ADP (in the case of the RMPFK-lig structure), or ATP (RMPFK-ATP structure). X-ray diffraction data were recorded at 100 K on beamline BW7B of the European Molecular Biology Laboratory at the DORIS Storage Ring (DESY) and were processed with the HKL package.[30] The diffraction data are summarized in Table 1.

Structure solution and refinement

The structures of RMPFK were solved by MR with Phaser,[50] using the α subunit of *Sc*PFK as starting model. Solutions were found to correspond to two RMPFK subunits in the asymmetric unit. Initial electron density maps were subjected to density modification with non-crystallographic 2-fold averaging and solvent flattening, using DM.[46] Atomic models were refined using CNS[47] and validated with PROCHECK.[48] Electron density maps were as expected for a 3.2-Å resolution, and the $2F_o - F_c$ map is continuous for the main chain of the protein, although some side chains (mainly on the surface of the protein) have no visible density.

Accession numbers

Atomic coordinates and structure factors have been deposited in the PDB† under accession codes 3O8O (*Sc*PFK), 3O8N (RMPFK-lig), and 3O8L (RMPFK-ATP).

Acknowledgements

This work was supported by grants from the Ministry for Science and Higher Education (Poland; 3P04A-03625 and 2P04A-0629), DFG (KO1178/5-1), and EU Structural Funds (WND-POIG.01.03.02-00-006/08 and WND-POIG.01.03.02-00-005/08). T.R. was supported by the National Institutes of Health (R01 GM069551). S.H.C. acknowledges the Department of Biological Sciences and the College of Basic Sciences, Louisiana State University, for support, as well as M. Newcomer, G. Waldrop, S. Bartlett, and E. Hawkins for advice and discussion.

† http://www.pcsb.org

Supplementary Data

Supplementary data associated with this article can be found, in the online version, at doi:10.1016/j.jmb.2011.01.019

References

1. Fothergill-Gilmore, L. A. & Michels, P. A. (1993). Evolution of glycolysis. *Prog. Biophys. Mol. Biol.* **59**, 105–235.
2. Hofmann, E. & Kopperschläger, G. (1982). Phosphofructokinase from yeast. *Methods Enzymol.* **90**, 49–60.
3. Sols, A. (1981). Multimodulation of enzyme activity. *Curr. Top. Cell. Regul.* **19**, 77–101.
4. Pilkis, S. J., El-Maghrabi, M. R. & Claus, T. H. (1988). Hormonal regulation of hepatic gluconeogenesis and glycolysis. *Annu. Rev. Biochem.* **57**, 755–783.
5. Okar, D. A. & Lange, A. J. (1999). Fructose-2,6-bisphosphate and control of carbohydrate metabolism in eukaryotes. *Biofactors*, **10**, 1–14.
6. Poorman, R. A., Randolph, A., Kemp, R. G. & Heinrikson, R. L. (1984). Evolution of phosphofructokinase—gene duplication and creation of new effector sites. *Nature*, **309**, 467–469.
7. Dunaway, G. A. (1983). A review of animal phosphofructokinase isozymes with an emphasis on their physiological role. *Mol. Cell. Biochem.* **52**, 75–91.
8. Telford, J. N., Lad, P. M. & Hammes, G. G. (1975). Electron microscope study of native and crosslinked rabbit muscle phosphofructokinase. *Proc. Natl Acad. Sci. USA*, **72**, 3054–3056.
9. Hesterberg, L. K., Lee, J. C. & Erickson, H. P. (1981). Structural properties of an active form of rabbit muscle phosphofructokinase. *J. Biol. Chem.* **256**, 9724–9730.
10. Vértessy, B. G., Kovács, J. & Ovádi, J. (1996). Specific characteristics of phosphofructokinase–microtubule interactions. *FEBS Lett.* **379**, 191–195.
11. Silva, A. P., Alves, G. G., Araujo, A. H. & Sola-Penna, M. (2004). Effects of insulin and actin on phosphofructokinase activity and cellular distribution in skeletal muscle. *An. Acad. Bras. Cienc.* **76**, 541–548.
12. Chaffotte, A. F., Laurent, M., Tijane, M., Tardieu, A., Roucous, C., Seydoux, F. *et al.* (1984). Studies on the structure of yeast phosphofructokinase. *Biochimie (Paris)*, **66**, 49–58.
13. Kopperschläger, G., Bär, J., Nissler, K. & Hofmann, E. (1977). Physicochemical parameters and subunit composition of yeast phosphofructokinase. *Eur. J. Biochem.* **81**, 317–325.
14. Heinisch, J., Ritzel, R. G., von Borstel, R. C., Aguilera, A., Rodicio, R. & Zimmermann, F. K. (1989). The

phosphofructokinase genes of yeast evolved from two duplication events. *Gene*, **78**, 309–321.
15. Li, Y., Rivera, D., Ru, W., Gunasekera, D. & Kemp, R. G. (1999). Identification of allosteric sites in rabbit phosphofructo-1-kinase. *Biochemistry*, **38**, 16407–16412.
16. Evans, P. R. & Hudson, P. J. (1979). Structure and control of phosphofructokinase from *Bacillus stearothermophilus*. *Nature*, **279**, 500–504.
17. Evans, P. R., Farrants, G. W. & Hudson, P. J. (1981). Phosphofructokinase: structure and control. *Philos. Trans. R. Soc. London Ser. B*, **293**, 53–62.
18. Shirakihara, Y. & Evans, P. R. (1988). Crystal structure of the complex of phosphofructokinase from *Escherichia coli* with its reaction products. *J. Mol. Biol.* **204**, 973–994.
19. Rypniewski, W. R. & Evans, P. R. (1989). Crystal structure of unliganded phosphofructokinase from *Escherichia coli*. *J. Mol. Biol.* **207**, 805–821.
20. Schirmer, T. & Evans, P. R. (1990). Structural basis of the allosteric behaviour of phosphofructokinase. *Nature*, **343**, 140–145.
21. Parmeggiani, A., Luft, J. H., Love, D. S. & Krebs, E. G. (1966). Crystallization and properties of rabbit skeletal muscle phosphofructokinase. *J. Biol. Chem.* **241**, 4625–4637.
22. Ruiz, T., Kopperschläger, G. & Radermacher, M. (2001). The first three-dimensional structure of phosphofructokinase from *Saccharomyces cerevisiae* determined by electron microscopy of single particles. *J. Struct. Biol.* **136**, 167–180.
23. Ruiz, T., Mechin, I., Bär, J., Rypniewski, W., Kopperschläger, G. & Radermacher, M. (2003). The 10.8-Å structure of *Saccharomyces cerevisiae* phosphofructokinase determined by cryoelectron microscopy: localization of the putative fructose 6-phosphate binding sites. *J. Struct. Biol.* **143**, 124–134.
24. Bárcena, M., Radermacher, M., Bär, J., Kopperschläger, G. & Ruiz, T. (2007). The structure of the ATP-bound state of *S. cerevisiae* phosphofructokinase determined by cryo-electron microscopy. *J. Struct. Biol.* **159**, 135–143.
25. Martinez-Oyanedel, J., McNae, I. W., Nowicki, M. W., Keillor, J. W., Michels, P. A., Fothergill-Gilmore, L. A. *et al.* (2007). The first crystal structure of phosphofructokinase from a eukaryote: *Trypanosoma brucei*. *J. Mol. Biol.* **366**, 1185–1198.
26. Sträter, N., Marek, S., Kuettner, E. B., Kloos, M., Keim, A., Brüser, A. *et al.* (2010). Molecular architecture and structural basis of allosteric regulation of eukaryotic phosphofructokinases. *FASEB J.* **25**, 89–98.
27. Obmolova, G., Kopperschläger, G., Heinisch, J. & Rypniewski, W. R. (1998). Crystallization and preliminary X-ray analysis of the 12S form of phosphofructokinase from *Saccharomyces cerevisiae*. *Acta Crystallogr. Sect. D*, **54**, 96–98.
28. Kopperschläger, G., Bär, J. & Stellwagen, E. (1993). Limited proteolysis of yeast phosphofructokinase. Sequence locations of cleavage sites created by the actions of different proteinases. *Eur. J. Biochem.* **217**, 527–533.
29. Valaitis, A. P., Foe, L. G. & Kemp, R. G. (1987). Desensitization of muscle phosphofructokinase to ATP inhibition by removal of carboxyl-terminal heptadecapeptide. *J. Biol. Chem.* **262**, 5044–5048.
30. Otwinowski, Z. & Minor, W. (1997). Processing of X-ray diffraction data collected in oscillation mode. *Methods Enzymol.* **276**, 307–326.
31. Evans, P. R. (2006). Scaling and assessment of data quality. *Acta Crystallogr. Sect. D*, **62**, 72–82.
32. Kelley, E. L., Voll, R. J., Voll, V. A. & Younathan, E. S. (1986). Stereospecificity of the fructose 2,6-bisphosphate site of muscle 6-phosphofructo-1-kinase. *Biochemistry*, **25**, 1245–1248.
33. Ishikawa, E., Ogushi, S., Ishikawa, T. & Uyeda, K. (1990). Activation of mammalian phosphofructokinases by ribose 1,5-bisphosphate. *J. Biol. Chem.* **265**, 18875–18878.
34. Kemp, R. G. & Foe, L. G. (1983). Allosteric regulatory properties of muscle phosphofructokinase (Review). *Mol. Cell. Biochem.* **57**, 147–154.
35. Bock, P. E. & Frieden, C. (1976). Phosphofructokinase: I. Mechanism of the pH-dependent inactivation and reactivation of the rabbit muscle enzyme. *J. Biol. Chem.* **251**, 5630–5636.
36. Li, J., Zhu, X., Byrnes, M., Nelson, J. W. & Chang, S. H. (1993). Site-directed mutagenesis of rabbit muscle phosphofructokinase cDNA. Mutations at glutamine 200 affect the allosteric properties of the enzyme. *J. Biol. Chem.* **268**, 24599–24606.
37. Chang, S. H. & Kemp, R. G. (2002). Role of Ser530, Arg292, and His662 in the allosteric behavior of rabbit muscle phosphofructokinase. *Biochem. Biophys. Res. Commun.* **290**, 670–675.
38. Ferreras, C., Hernández, E. D., Martínez-Costa, O. H. & Aragón, J. J. (2009). Subunit interactions and composition of the fructose 6-phosphate catalytic site and the fructose 2,6-bisphosphate allosteric site of mammalian phosphofructokinase. *J. Biol. Chem.* **284**, 9124–9131.
39. Nakajima, H., Raben, N., Hamaguchi, T. & Yamasaki, T. (2002). Phosphofructokinase deficiency; past, present and future. *Curr. Mol. Med.* **2**, 197–212.
40. Kemp, R. G. & Gunasekera, D. (2002). Evolution of the allosteric sites of mammalian phosphofructo-1-kinase. *Biochemistry*, **41**, 9426–9430.
41. Uyeda, K. (1979). Phosphofructokinase. *Adv. Enzymol. Relat. Areas Mol. Biol.* **48**, 193–244.
42. Seeboth, P. G., Bohnsack, K. & Hollenberg, C. P. (1990). Pdc1(0) mutants of *Saccharomyces cerevisiae* give evidence for an additional structural PDC gene: cloning of PDC5, a gene homologous to PDC1. *J. Bacteriol.* **172**, 678–685.
43. Bär, J., Huse, K., Kopperschläger, G., Behlke, J. & Schultz, W. (1988). Phosphofructokinase from baker's yeast: properties of a proteolytically modified active enzyme form. *Int. J. Biol. Macromol.* **10**, 99–105.
44. Navaza, J. (1994). AMoRe: an automated package for molecular replacement. *Acta Crystallogr. Sect. A*, **50**, 157–163.
45. Collaborative Computational Project, Number 4. (1994). The CCP4 suite: programs for protein crystallography. *Acta Crystallogr. Sect. D*, **50**, 760–763.
46. Cowtan, K. (1994). 'DM': an automated procedure for phase improvement by density modification. *Jt. CCP4 ESF-EACBM Newsl. Protein Crystallogr.* **31**, 34–38.

47. Brünger, A. T., Adams, P. D., Clore, G. M., DeLano, W. L., Gros, P., Grosse-Kunstleve, R. W. *et al.* (1998). Crystallography and NMR system: a new software suite for macromolecular structure determination. *Acta Crystallogr. Sect. D*, **54**, 905–921.
48. Laskowski, R. A., MacArthur, M. W., Moss, D. S. & Thornton, J. M. (1993). PROCHECK: a program to check the stereochemical quality of protein structures. *J. Appl. Crystallogr.* **26**, 283–291.
49. Luft, J. R., Collins, J. R., Fehrman, N. A., Lauricella, A. M., Veatch, C. K. & DeTitta, G. T. (2003). A deliberate approach to screening for initial crystallizations of biological macromolecules. *J. Struct. Biol.* **142**, 170–179.
50. McCoy, A. J., Grosse-Kunstleve, R. W., Adams, P. D., Winn, M. D., Storoni, L. C. & Read, R. J. (2007). Phaser crystallographic software. *J. Appl. Crystallogr.* **40**, 658–674.